Electron-impact-induced allowed transitions between triplet states of H_2

A. Laricchiuta
IMIP CNR, Sezione territoriale di Bari, Bari, Italy

R. Celiberto
DICA–Dipartimento di Ingegneria Civile e Ambientale, Politecnico di Bari, Bari, Italy

R. K. Janev*
Macedonian Academy of Sciences and Arts, Skopje, Macedonia

(Received 21 December 2002; revised manuscript received 29 October 2003; published 17 February 2004)

Electron-impact-induced excitation and dissociation processes between the excited triplet states $a\,^3\Sigma_g^+ \rightarrow d\,^3\Pi_u$, $c\,^3\Pi_u \rightarrow h\,^3\Sigma_g^+$, and $c\,^3\Pi_u \rightarrow g\,^3\Sigma_g^+$ of molecular hydrogen are studied by using the impact-parameter method. The cross sections for $\nu_i - \nu_f$ resolved vibronic transitions between states have been calculated in the energy range from threshold to 100 eV; their maxima being located in the region of 5–10 eV. A special treatment was required for the transition to the $h\,^3\Sigma_g^+$ state, whose adiabatic potential-energy curve possesses a barrier at the internuclear distance of about $5a_0$, sustaining three quasi-bound vibrational states with widths of 5.3×10^{-12}, 1.5×10^{-3}, and 42.0 cm^{-1}, respectively. The quasistationary character of these vibrational states is taken into account when calculating the $c\,^3\Pi_u \rightarrow h\,^3\Sigma_g^+$ excitation and dissociation cross sections.

DOI: 10.1103/PhysRevA.69.022706 PACS number(s): 34.80.Gs, 34.80.Ht, 52.20.Hv, 33.70.Ca

I. INTRODUCTION

The electron-impact excitation and dissociation collisions of vibrationally excited hydrogen molecules, either in their ground or excited bound electronic states, play an important role in the kinetics of many astrophysical and laboratory hydrogen containing low-temperature plasmas [1]. The determination of electron energy distribution function and molecular vibrational temperature, and the interpretation of many spectroscopic and transport properties of such plasmas require knowledge of electron-impact excitation (and dissociation) cross sections resolved in both the initial and final vibrational states [2].

There have been a significant number of excitation (and dissociative excitation) cross-section calculations for transitions from vibrationally excited H_2 in its ground electronic state [3], and only one of these calculations has included two electronically excited states of H_2 [4]. With the exception of Refs. [5–9], all these calculations were performed for transitions involving singlet electronic states. Total excitation cross sections have, however, been done in Ref. [10] for transitions from the ground vibrational state of $H_2(X\,^1\Sigma_g^+)$ to triplet $b\,^3\Sigma_u^+$, $c\,^3\Pi_u$, $a\,^3\Sigma_g^+$, $d\,^3\Pi_u$, and $e\,^3\Sigma_u^+$ states.

Recently, a diagnostic method has been applied for determination of plasma electron temperature and vibrational temperature of $H_2(X\,^1\Sigma_g^+)$ in low-temperature (0.5–5 eV) technical and fusion divertor plasmas [11,12]. The method is based on the intensity measurement of the $\nu_i - \nu_f$ resolved transitions in the Fulcher band ($a\,^3\Sigma_g^+ \rightarrow d\,^3\Pi_u$) of the H_2 molecule. A full development of this method requires cross section information on all population and depopulation processes involving $a(^3\Sigma_g^+, \nu_i)$ and $d(^3\Pi_u, \nu_f)$, as well as those for the states $c\,^3\Pi_u$, $h\,^3\Sigma_g^+$, $g\,^3\Sigma_g^+$, $i\,^3\Pi_g$, and $j\,^3\Delta_g$, to which $a\,^3\Sigma_g^+$ and $d\,^3\Pi_u$ are strongly coupled.

In the present work we shall study the dipole-allowed $a\,^3\Sigma_g^+ \rightarrow d\,^3\Pi_u$, $c\,^3\Pi_u \rightarrow h\,^3\Sigma_g^+$, and $c\,^3\Pi_u \rightarrow g\,^3\Sigma_g^+$, transitions as they are the strongest ones that couple the $n=2$ (a,c) and $n=3$ (h,e,d,g,i,j) groups of states, where n is the state's principal quantum number in the united atom limit. The $\nu_i - \nu_f$ resolved excitation and ν_i resolved dissociative excitation cross sections will be calculated by using the impact-parameter method [13–15], employed previously in many similar calculations for the transitions within the series of singlet electronic states of H_2 [4,14–18]. The c-h triplet system is different from the a-d and c-g, and from all previously studied singlet-singlet systems, in that the adiabatic potential-energy curve of the $h\,^3\Sigma_g^+$ state has a potential barrier at internuclear distances of about $5.0a_0$, where a_0 is the Bohr radius. The three uppermost vibrational states in this potential lie above the dissociation limit of $h\,^3\Sigma_g^+$ state, and have, therefore, a quasibound nature. Transitions to these quasistationary states will require a special attention and treatment.

The organization of our paper is as follows: in Sec. II we briefly outline the employed computational method. In Sec. III we give some of the computational details, while in Secs. IV and V the results are presented and discussed. Finally the summary and conclusions are given in Sec. VI.

II. METHOD OF CROSS-SECTION CALCULATIONS

The basic idea of impact-parameter method (IPM) consists in classical description of incident electron motion (for which a straight-line trajectory is assumed) and quantum-

*Present address: Institute of Plasma Physics, Forschungszentrum-Juelich, Juelich, Germany.

mechanical description of molecular (both electronic and nuclear) motions. Implicit to this method is the assumption of dominance of ''distant collisions'' and the constraint on impact-parameter values to be larger than the typical molecular dimensions (to avoid overlap effects with the molecular cloud, which would require a quantum description of the incident electron motion).

In this approach, the electron-target interaction potential is a time-dependent function, and, consequently, the collisional dynamics is described by a time-dependent Schrödinger equation [19].

The impact-parameter method is a two-state, perturbative method which at high energies reduces to the Born approximation.

In the context of present calculations, which involve a group of energetically close-lying and coupled electronic states, a close-coupling approach to the collision dynamics of considered processes would certainly be much more appropriate. This is particularly true for the dynamics at intermediate and low collision energies (corresponding to the collision energy region around the cross-section maximum and below). However, the practical implementation of such an approach would require inclusion in the expansion basis also of the states from the $n=4$ (and even higher n) manifold, in order to accurately describe the transitions within the $n=2$ and $n=3$ manifolds. Inclusion of high vibrational states in such an approach would also lead to a significant extension of the configuration space in which the couplings are strong, and, consequently, to serious numerical (convergence) difficulties. Nevertheless, the multistate coupling nature of $n=2$ and $n=3$ collision dynamics remains, and its reduction to sets of isolated two-state dipole couplings (as inherent to the first-order methods, such as IPM) is an approximation that can be justified only at energies considerably higher than the transition energy involved.

No data are available in literature for comparison for these transitions. However, the cross-section results obtained in the two-state theoretical frame for transitions between singlet Rydberg states of the hydrogen molecule have proved to be fairly reliable [18]. These highly excited electronic states, like those in the triplet series, are embedded in the H_2 electronic manifold (and, accordingly, coupled via many dipole-allowed transitions), yet the discrepancy between the calculated cross sections and the available $\nu_i=0$ experimental data was found to be within a factor 2, in the worse case. This seems to indicate that first-order methods can give a semiquantitative information on cross-section magnitude. This work can be considered a step forward in understanding the dynamics of triplet states, which, to our best knowledge, have been still very little studied either experimentally or theoretically.

In this frame, some general qualitative argument can help us to elucidate the coupling dynamics of triplet electronic states considered here. For dipole-allowed triplet-triplet transitions, the coupling is provided by their transition dipole moment $|M_{if}|$ as a function of the internuclear distance R [see Eq. (2) below]. The *a*, *c*, *h*, *d*, and *g* states, involved in the transitions considered here, are also coupled with other triplet states (e.g., $e\,^3\Sigma_u^+$, $i\,^3\Sigma_g^+$, etc.), particularly those

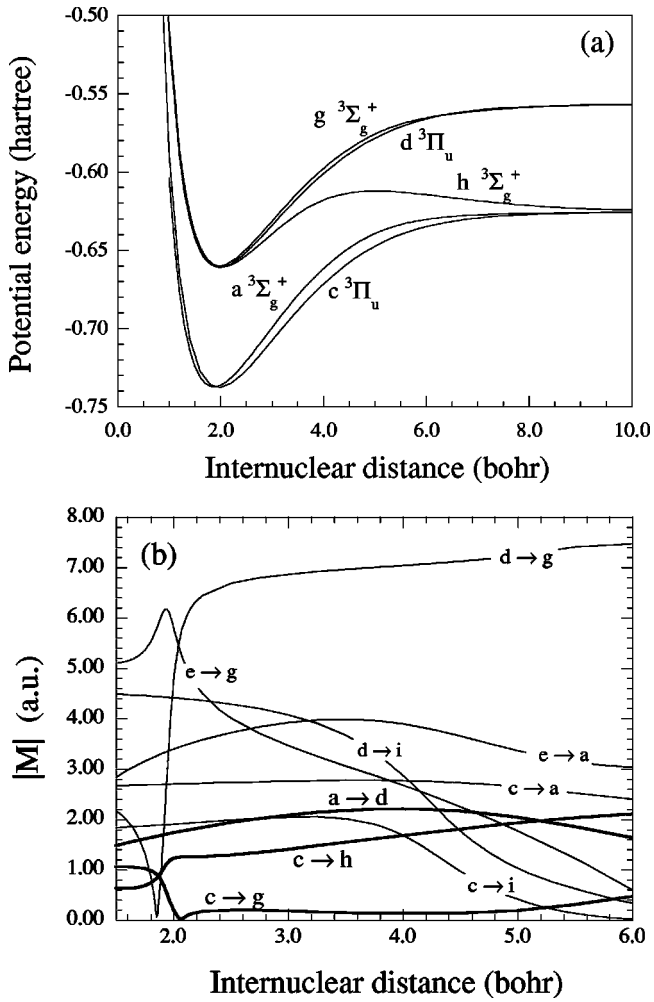

FIG. 1. (a) Schematic energy diagram for triplet states of H_2 molecule; (b) transition dipole moment as a function of internuclear distance for some triplet-triplet transitions (thick lines indicate the transitions considered in this paper).

that energetically lie close to them. The potential-energy curves of $n=2$ and some $n=3$ triplet states (taken from Ref. [20]), and the dipole moments $|M_{if}(R)|$ for the considered $a\,^3\Sigma_g^+ \rightarrow d\,^3\Pi_u$, $c\,^3\Pi_u \rightarrow h\,^3\Sigma_g^+$, and $c\,^3\Pi_u \rightarrow g\,^3\Sigma_g^+$ and some other transitions (taken from Ref. [20]) are shown in Figs. 1(a) and 1(b), respectively. While $|M_{if}(R)|$ is the relevant parameter expressing the strength of the coupling between $|i\rangle$ and $|f\rangle$ states, the *R*-extension of this coupling is determined by the overlap of the vibrational wave functions of initial and final electronic states [see Eq. (2) below]. From Fig. 1(b) it can be seen that in the range $\sim 1.5a_0$–$6.0a_0$ of *R*, where majority of vibrational states of considered $n=2$ and $n=3$ electronic states are localized, the dipole moments for $a\,^3\Sigma_g^+ \rightarrow d\,^3\Pi_u$, $c\,^3\Pi_u \rightarrow h\,^3\Sigma_g^+$, and $c\,^3\Pi_u \rightarrow g\,^3\Sigma_g^+$ transitions are significantly smaller than those for other transitions (e.g., $e\,^3\Sigma_u^+ \rightarrow a\,^3\Sigma_g^+$, $d\,^3\Pi_u \rightarrow g\,^3\Sigma_g^+$). The large difference between the dipole moments for different transitions as well as the $g \leftrightarrow u$ selection rules facilitate an approximate decoupling of the dynamics of *strongly* coupled states from that of *weakly* coupled states. For instance, the dynamics of strongly coupled (but pairwise) *a*, *c*, *e*, and *g* states is not significantly

affected by the weak couplings of $a \rightarrow d$, $c \rightarrow h$, and $c \rightarrow g$ pairs of states. Conversely, when considering the $a \rightarrow d$, $c \rightarrow h$, and $c \rightarrow g$ transitions the initial-state amplitudes can be considered as predetermined by their strong-coupling dynamics with the other states or, in other words, the time scale on which the strong transitions take place is much shorter than that for the weak transitions, resulting in separation of their dynamics. Finally, the considered transitions are symmetry decoupled, and each of them can be considered separately as a two-state dynamical problem.

In the following we give a brief account of the main elements of IPM computational scheme, referring the reader to the literature for a complete description of the method [13–15].

The state-to-state cross section $\sigma_{\nu_i,\nu_f}^{\alpha_i \rightarrow \alpha_f}(E)$ for an electron-impact-induced transition from the ν_ith vibrational level of the α_i electronic state to the ν_fth vibrational level of the final α_f electronic state of a diatomic molecule is expressed, in the IPM framework, as

$$\sigma_{\nu_i,\nu_f}^{\alpha_i \rightarrow \alpha_f}(E) = S_{\nu_i,\nu_f}^{\alpha_i,\alpha_f} D_{\nu_i,\nu_f}^{\alpha_i,\alpha_f}(E), \tag{1}$$

where E is the incident kinetic energy. The ''structural factor'' $S_{\nu_i,\nu_f}^{\alpha_i,\alpha_f}$, related to the target structure, is defined by

$$S_{\nu_i,\nu_f}^{\alpha_i,\alpha_f} = \frac{m^2 e^2}{3 g_i \hbar^4} (2 - \delta_{\Lambda_i,0})(2 - \delta_{\Lambda_f,0}) \times \left| \int_0^\infty dR \chi_{\nu_f}^{\alpha_f}(R) M_{\Lambda_i,\Lambda_f}^{\alpha_i,\alpha_f}(R) \chi_{\nu_i}^{\alpha_i}(R) \right|^2. \tag{2}$$

In this expression m, e, $\hbar$, and g_i represent, respectively, the mass and charge of electron, Planck's constant, and the degeneracy factor for the α_i state. $\chi_\nu^\alpha(R)$ is the vibrational wave function that depends on the internuclear distance R, and $M_{\Lambda_i,\Lambda_f}^{\alpha_i,\alpha_f}(R)$ is the usual electronic transition dipole moment characterized by the quantum numbers of the projection of electronic angular momentum on the internuclear axis Λ_i and Λ_f.

The ''dynamical factor'' $D_{\nu_i,\nu_f}^{\alpha_i,\alpha_f}(E)$ describing the inelastic-scattering effects on the motion of incident electron is given by

$$D_{\nu_i,\nu_f}^{\alpha_i,\alpha_f} = \frac{2\pi\hbar^2}{m^2 u_i^2} \left[\gamma_i \left(K_0(\gamma_i) K_1(\gamma_i) - \frac{\pi^2}{4} S_0(\gamma_i) S_1(\gamma_i) \right) + \gamma_f \left(K_0(\gamma_f) K_1(\gamma_f) - \frac{\pi^2}{4} S_0(\gamma_f) S_1(\gamma_f) \right) + \gamma \left(K_0(\gamma_i) K_1(\gamma_f) + K_0(\gamma_f) K_1(\gamma_i) + \frac{\pi^2}{4} S_0(\gamma_i) S_1(\gamma_f) + \frac{\pi^2}{4} S_0(\gamma_f) S_1(\gamma_i) \right) + \left(\frac{u_i^2 - u_f^2}{u_i^2 + u_f^2} \right) \left(\ln\left(\frac{\gamma_f}{\gamma_i} \right) + \frac{\pi}{2} \int_{\gamma_i}^{\gamma_f} S_0(\gamma) d\gamma \right) \right], \tag{3}$$

where K_i and S_i are the modified Bessel and Struve functions, respectively, and u_i and u_f are the initial and final electron velocities. Moreover

$$\gamma_i = \frac{\rho_{\nu_i,\nu_f}^0 |\Delta E_{\nu_i,\nu_f}^{\alpha_i,\alpha_f}|}{\hbar} \frac{1}{u_i}, \tag{4}$$

$$\gamma_f = \frac{\rho_{\nu_i,\nu_f}^0 |\Delta E_{\nu_i,\nu_f}^{\alpha_i,\alpha_f}|}{\hbar} \frac{u_i}{u_f^2}, \tag{5}$$

$$\gamma = \frac{\rho_{\nu_i,\nu_f}^0 |\Delta E_{\nu_i,\nu_f}^{\alpha_i,\alpha_f}|}{\hbar} \frac{2u_i}{u_i^2 + u_f^2}, \tag{6}$$

with $\Delta E_{\nu_i,\nu_f}^{\alpha_i,\alpha_f}$ being the transition energy defined as

$$\Delta E_{\nu_i,\nu_f}^{\alpha_i,\alpha_f} = \epsilon_{\nu_f}^{\alpha_f} - \epsilon_{\nu_i}^{\alpha_i} \tag{7}$$

and ϵ_ν^α is the energy eigenvalue of the νth vibrational level of the α electronic state. ρ_{ν_i,ν_f}^0, in Eqs. (4)–(6), is a cutoff parameter introduced in the impact-parameter method to preserve the unitary of S matrix [13–15], whose value is set by equating the impact-parameter and Born approximation cross sections at high energies.

The dissociative cross section $\sigma_{\nu_i}^{\alpha_i \rightarrow \alpha_f}(E)$ is defined by the integral

$$\sigma_{\nu_i}^{\alpha_i \rightarrow \alpha_f}(E) = \int_{\varepsilon_{th}}^{\varepsilon_{max}} \frac{d\sigma_{\nu_i,\varepsilon}^{\alpha_i \rightarrow \alpha_f}(E)}{d\varepsilon} d\varepsilon, \tag{8}$$

where $\sigma_{\nu_i,\varepsilon}^{\alpha_i \rightarrow \alpha_f}(E)$ is readily obtained from Eq. (1) by simply replacing the final quantum number ν_f with the continuum energy ε. The continuum integration limits ε_{th}, ε_{max} are, respectively, defined as

$$\varepsilon_{th} = V_{\alpha_f}(R \rightarrow \infty), \quad \varepsilon_{max} = E + \epsilon_{\nu_i}^{\alpha_i}. \tag{9}$$

Here $V_{\alpha_f}(R \rightarrow \infty)$ is the dissociation threshold for the upper α_f electronic state.

Finally the *total cross sections* can be written as

$$\sigma_{\nu_i}^{\alpha_i \rightarrow \alpha_f}(E) = \sum_{\nu_f} \sigma_{\nu_i,\nu_f}^{\alpha_i \rightarrow \alpha_f}(E) + \int_{\epsilon_{th}}^{\epsilon_{max}} d\epsilon \frac{d\sigma_{\nu_i,\epsilon}^{\alpha_i \rightarrow \alpha_f}(E)}{d\epsilon}, \tag{10}$$

where the sum extends over all the bound vibrational levels of the α_f state.

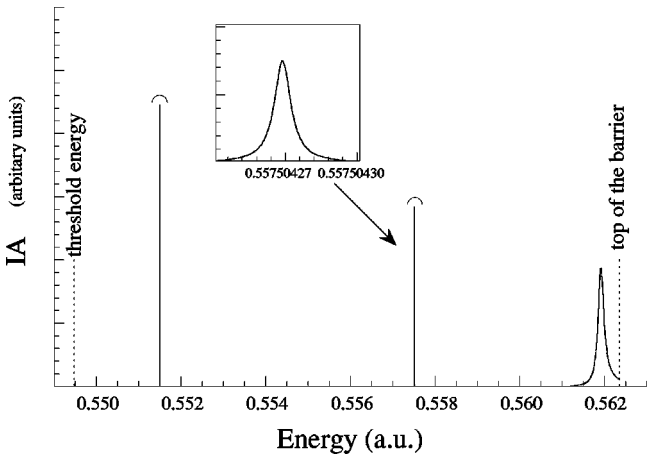

FIG. 2. Internal amplitude, Eq. (12), as a function of continuum energy (the second peak is magnified in the inserted picture).

III. COMPUTATIONAL DETAILS

A. Potential-energy curves, vibrational states, and determination of ρ_0

The potential-energy curves and transition dipole moments for the considered transitions, needed for calculation of the structural factor (2), were taken from literature [20] [see Figs. 1(a) and 1(b)]. The repulsive portion of the potential curves, at very short internuclear distances ($R<0.6a_0$), has been extrapolated by the analytical expression

$$V(R)=A\exp(-BR), \tag{11}$$

where the constants A and B have been determined by interpolation of the first two calculated points, corresponding to the shortest internuclear distances [14].

The discrete vibrational eigenvalues and wave functions were obtained by employing the Numerov numerical procedure, while vibrational wave functions belonging to the continuum of the final electronic state were calculated by using the method outlined in Ref. [17].

The Born cross sections at high collision energy, needed to determine the cutoff parameter ρ_0, were calculated in the usual fashion in terms of the generalized oscillator strength [4]. The electronic wave functions, needed in this last quantity, were obtained by performing full configuration interaction ab initio calculations with the GAMESS package [21]. In the range of $(0.6–6.0a_0)$ internuclear distances, was chosen a basis set of Gaussians $(8s,4p,3d)$ contracted to $[4s,3p,2d]$ [22,23] and augmented by the Rydberg-like s (exponential parameter $\zeta=0.01$), p ($\zeta=0.03$, 0.01), d ($\zeta=1.0$, 0.03, 0.01), f ($\zeta=0.03$, 0.01) functions on the center of mass [24]; for $R>6.0a_0$ the basis set was enriched with four diffuse d functions ($\zeta=0.197$, 0.079, 0.032, 0.013) [25]. Potential-energy curves for excited triplet states, as well as transition dipole moments, were found to be in good agreement with Ref. [20] in the range $(0.6–8.0a_0)$. Due to the lack of accuracy in reproducing electronic state energy in the asymptotic region ($R>8.0a_0$), the cross section calculations were performed only for $\nu_i\leqslant 13$.

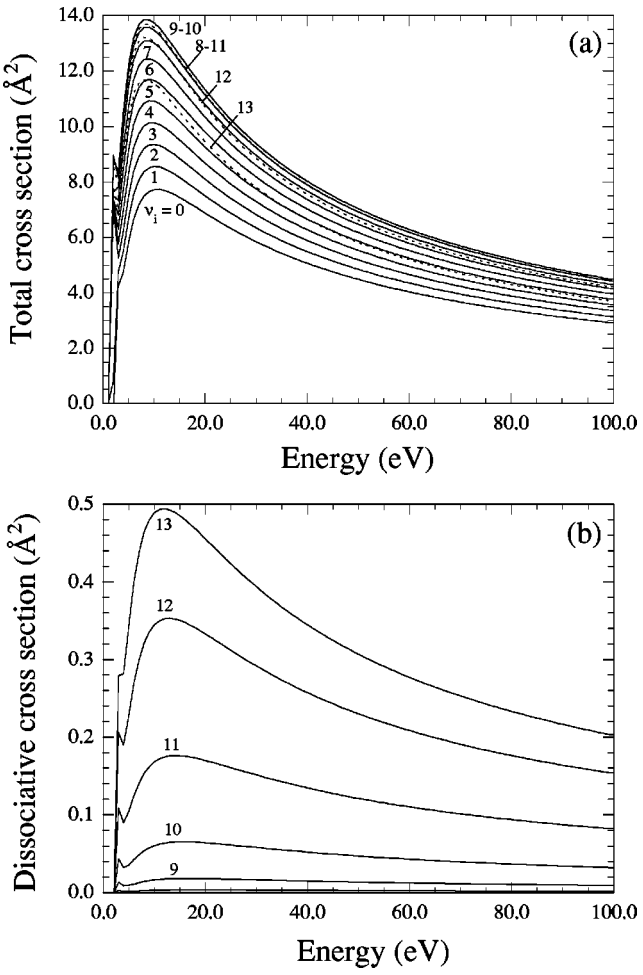

FIG. 3. Cross sections as a function of energy for the processes (a) $H_2(a\,^3\Sigma_g^+,\nu_i=0-13)+e\rightarrow H_2(d\,^3\Pi_u)+e$; (b) $H_2(a\,^3\Sigma_g^+,\nu_i=0-13)+e\rightarrow H_2(d\,^3\Pi_u)+e\rightarrow H+H+e$.

Finally in all the processes considered, due to the relative position of potential-energy curves coupled in the transition, the last vibrational levels of the initial electronic state are placed at higher energy with respect to the first levels of the final electronic states. In this case a vibrational deexcitation may occur in the electronic transition. We have not considered this possibility in our calculations.

B. Quasibound vibrational states

As already mentioned earlier, due to the existence of both a minimum and a maximum in the potential-energy curve of the $h\,^3\Sigma_g^+$ state, quasibound levels arise near the top of the potential barrier, which qualitatively correspond to vibrational levels of the diatomic system, but are unstable to tunneling through the potential barrier to the dissociation continuum. There are different procedures for determining the energies and widths of these quasibound levels (resonances) through the localization of maxima of the *collisional time delay function* τ, or treating the resonances as bound levels with discrete outer boundary condition (*Airy function boundary condition*) [26,27].

In the present work the energy positions of quasibound vibrational states were determined by using the method of

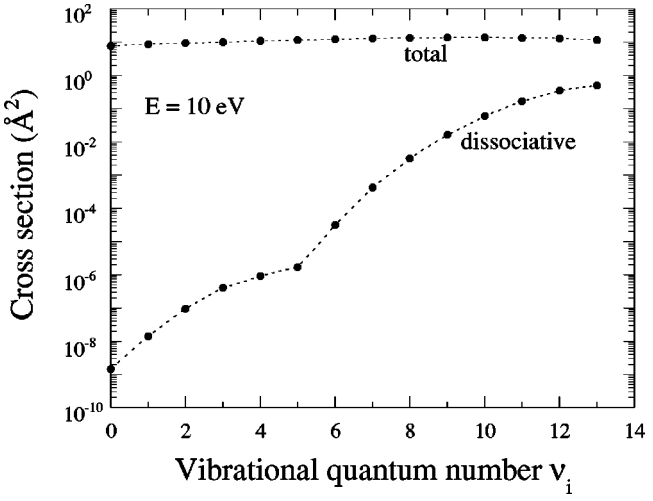

FIG. 4. Total [process (a) in the text] and dissociative [process (b)] cross sections as a function of initial vibrational quantum number at the collision energy $E=10$ eV.

internal amplitude (IA) given by

$$\mathrm{IA}(\varepsilon)=\int_{R_a}^{R_b}\frac{|\chi_\varepsilon(R)|^2 dR}{[R_b-R_a]}, \tag{12}$$

where R_a and R_b are the first two classical turning points of the vibrational level of energy ε and the vibrational wave function $\chi_\varepsilon(R)$ is asymptotically normalized according to Ref. [17]. The resonance energy positions correspond to the IA maxima.

In order to completely resolve the resonance spectrum from the threshold energy up to the barrier's maximum, we adopted an adaptative step size procedure [28], finding three quasibound vibrational states (see Fig. 2). The dissociating lifetime τ_d of these levels has been obtained in terms of the resonance dissociation width Γ through the relation

$$\tau_d=\frac{\hbar}{\Gamma}. \tag{13}$$

The parameter Γ has been estimated by the standard WKB semiclassical method [29], which gives

$$\Gamma^{WKB}=\frac{e^{-2\theta}}{2\phi'}, \tag{14}$$

where

$$\theta=\int_{R_b}^{R_c} dR(2\mu[V(R)-E]^{1/2}), \tag{15}$$

$$\phi=\int_{R_a}^{R_b} dR(2\mu[E-V(R)]^{1/2}), \tag{16}$$

R_c is the outer classical turning point.

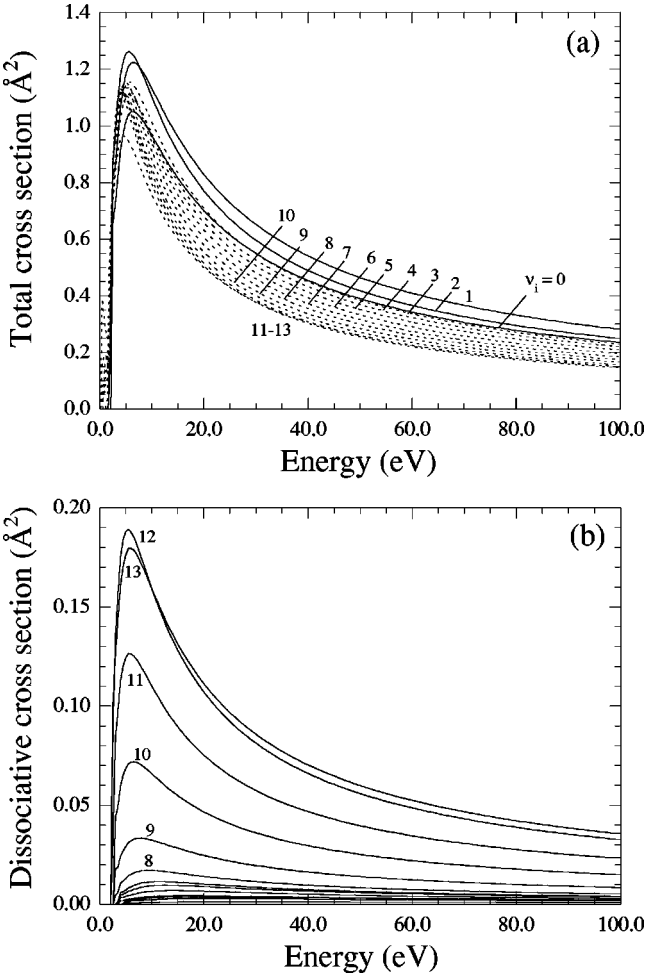

FIG. 5. Cross sections as a function of energy for the processes (a) $H_2(c\,^3\Pi_u,\nu_i=0-13)+e\rightarrow H_2(g\,^3\Sigma_g^+)+e$; (b) $H_2(c\,^3\Pi_u,\nu_i=0-13)+e\rightarrow H_2(g\,^3\Sigma_g^+)+e\rightarrow H+H+e$.

IV. RESULTS

A. Total and dissociative cross sections

Total excitation cross sections, for the process (a)

$$H_2(a\,^3\Sigma_g^+,\nu_i)+e\rightarrow H_2(d\,^3\Pi_u)+e$$

calculated by Eq. (10), are shown in Fig. 3(a) as a function of the incident energy. Each curve is identified by the value of the initial quantum number ν_i. The maxima of the cross sections monotonically increase by a factor of 2 from $\nu_i=0$ up to $\nu_i=9-10$ (solid lines), and decrease for $\nu_i>10$ (dashed lines). This trend, observed also in other cases [16,18], is mainly determined by the structural factor and it does not depend on the incident energy. The small peak appearing at very low energies is an artifact of the computational method. Figure 3(b) shows the dissociative cross sections as a function of the energy, obtained by Eq. (8), for the transition (b)

$$H_2(a\,^3\Sigma_g^+,\nu_i)+e\rightarrow H_2(d\,^3\Pi_u)+e\rightarrow H+H+e.$$

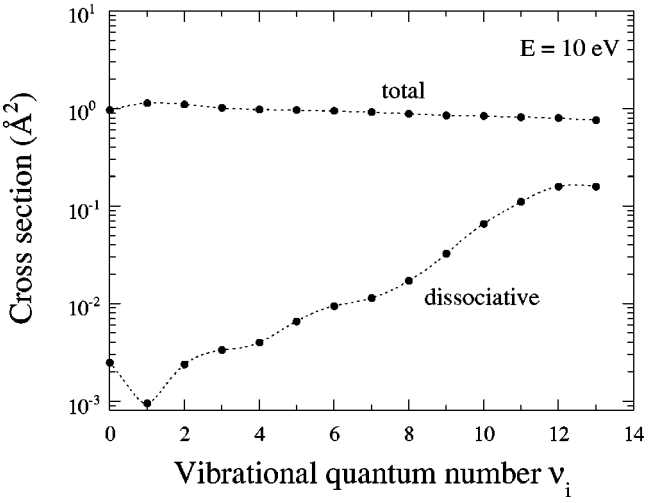

FIG. 6. Total [process (c) in the text] and dissociative [process (d)] cross sections as a function of initial vibrational quantum number at the collision energy $E=10$ eV.

The cross sections display a regular increase with the increase of vibrational level up to $\nu_i=13$, for which they reach their maximum. However they remain quite a small fraction of the total cross sections shown in Fig. 3(a). This point can be better appreciated in Fig. 4 where total and dissociative cross sections are compared as a function of the initial vibrational quantum number for a fixed incident electron energy of 10 eV (about the maximum of $\nu_i=0$ cross section).

Figures 5(a) and (b) show the total and dissociative cross sections for the processes (c) and (d)

$$H_2(c\,^3\Pi_u,\nu_i)+e\rightarrow H_2(g\,^3\Sigma_g^+)+e,$$

$$H_2(c\,^3\Pi_u,\nu_i)+e\rightarrow H_2(g\,^3\Sigma_g^+)+e\rightarrow H+H+e,$$

respectively. For $\nu_i>1$, and for an incident energy greater than 10 eV, the total cross sections decrease with the increase of vibrational quantum number (dashed lines). The dissociative cross sections of Fig. 5(b) give a very small contribution to the total cross sections also in this case. A comparison between total and dissociative cross sections is shown in Fig. 6 as a function of the vibrational quantum number for an incident electron energy of 10 eV.

Total and direct dissociative cross sections have been calculated also for the processes (e) and (f)

$$H_2(c\,^3\Pi_u,\nu_i)+e\rightarrow H_2(h\,^3\Sigma_g^+)+e,$$

$$H_2(c\,^3\Pi_u,\nu_i)+e\rightarrow H_2(h\,^3\Sigma_g^+)+e\rightarrow H+H+e,$$

and the results are shown in Figs. 7(a) and 7(b), respectively. The dependence of cross section on the vibrational levels for the above two processes is shown in Fig. 8 at a collision energy of 10 eV. For $\nu_i>4$ the dissociative cross section increases with the increasing of the vibrational quantum number, becoming the predominate contribution to the total cross section for $\nu_i\gtrsim 8$. The main feature of the $c\,^3\Pi_u \rightarrow h\,^3\Sigma_g^+$ transition is the existence, in the $h\,^3\Sigma_g^+$ electronic state, of three quasibound vibrational levels and the calcula-

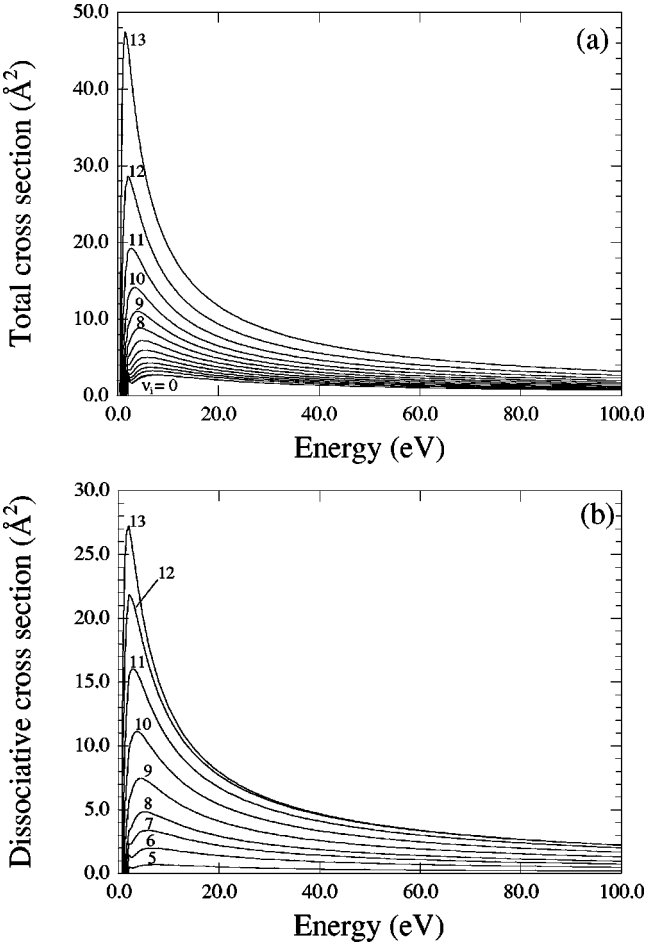

FIG. 7. Cross sections as a function of energy for the processes (a) $H_2(c\,^3\Pi_u,\nu_i=0-13)+e\rightarrow H_2(h\,^3\Sigma_g^+)+e$; (b) $H_2(c\,^3\Pi_u,\nu_i=0-13)+e\rightarrow H_2(h\,^3\Sigma_g^+)+e\rightarrow H+H+e$.

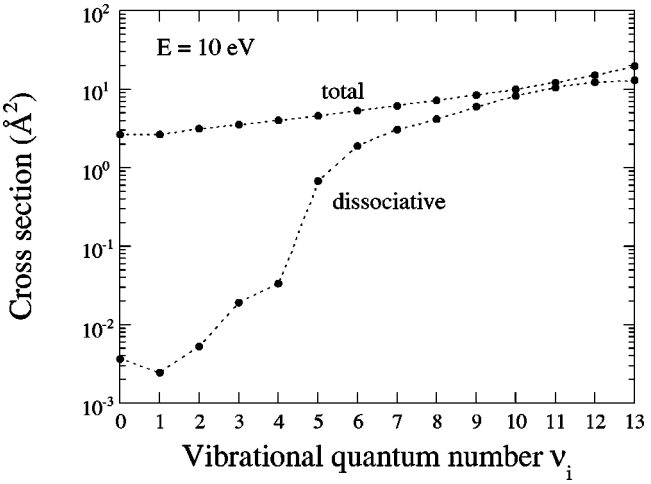

FIG. 8. Total [process (e) in the text] and dissociative [process (f)] cross sections as a function of initial vibrational quantum number at the collision energy $E=10$ eV.

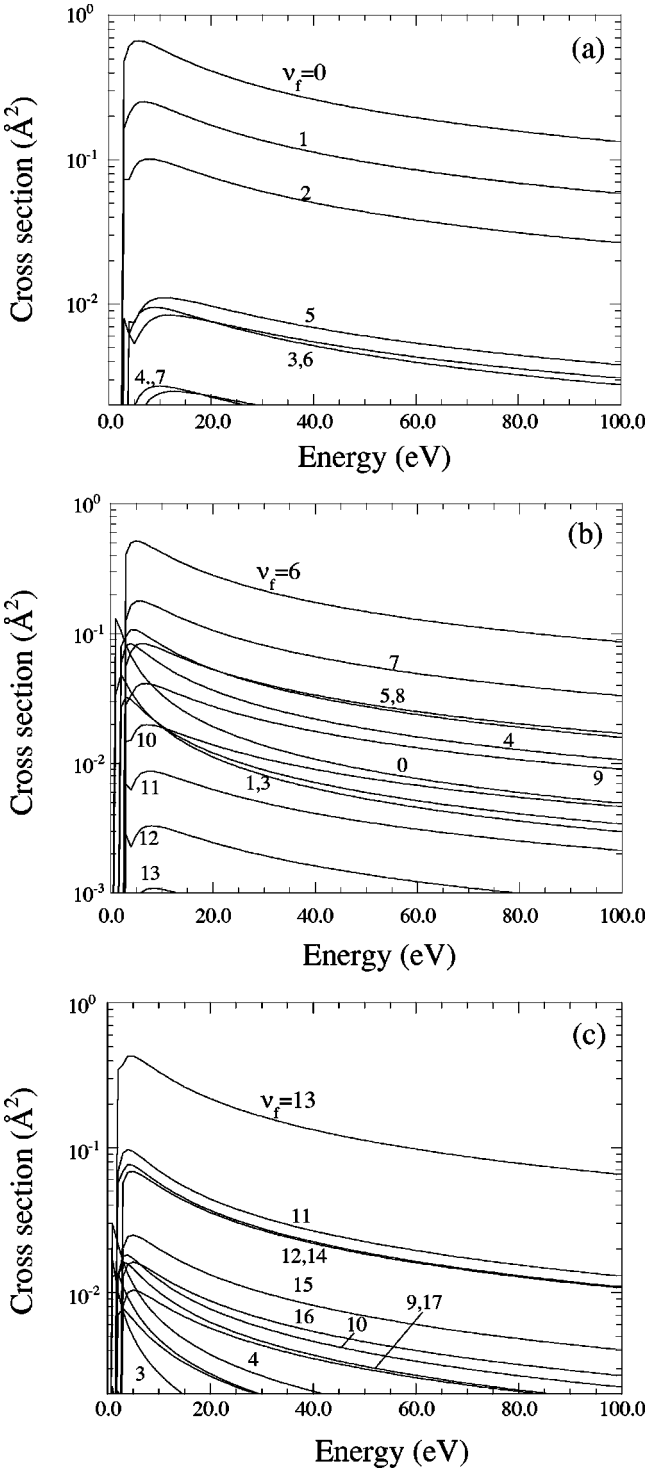

FIG. 9. State-to-state cross sections for process $H_2(c\,^3\Pi_u,\nu_i)+e\rightarrow H_2(g\,^3\Sigma_g^+,\nu_f)+e$ as a function of incident energy for different final vibrational levels ν_f and for (a) $\nu_i=0$, (b) $\nu_i=6$, (c) $\nu_i=13$.

tion of cross section for dissociation from these levels required a special treatment. A detailed discussion is given in Sec. V.

B. State-to-state cross sections

Figures 9(a)–9(c) show an example of state-to-state cross sections [Eq. (1)] for the transition $c\,^3\Pi_u\rightarrow g\,^3\Sigma_g^+$ as a function of the incident energy. The cross section $\sigma_{\nu_i,\nu_f}^{c\rightarrow g}$ depends on both the initial and final quantum numbers. Figures 9(a)–9(c), display the cross sections for $\nu_i=0$, 6, 13, respectively, and for all the ν_f levels of $g\,^3\Sigma_g^+$ electronic state. Inspection of these figures show that the energy dependence of the cross sections is practically the same above $\sim$20 eV for all the vibrational levels. It is determined by the dynamical factor, which can be considered approximately independent of the vibrational level of the molecule, particularly at high energies [17,30]. On the contrary, the trend of the cross sections as a function of the final vibrational quantum number is strongly affected by the structural factor. This can be clearly seen in Fig. 10, where the same cross sections as in Figs. 9(a)–9(c) are shown as a function of the final vibrational quantum number at a fixed incident electron energy of 10 eV, along with the corresponding structural factors normalized to the first ν_f cross section value.

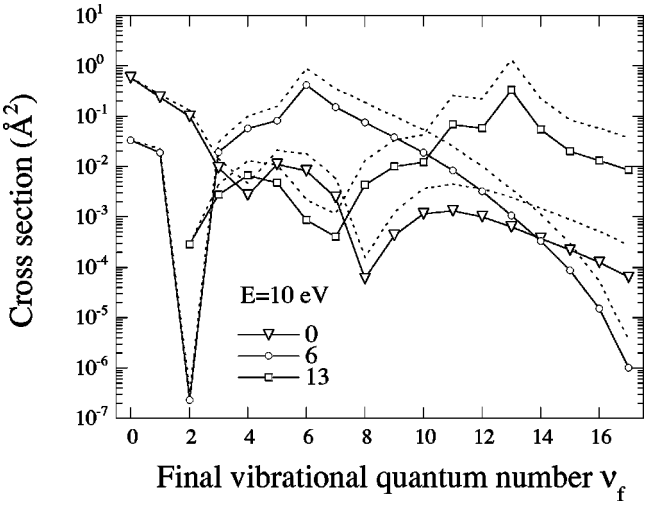

FIG. 10. State-to-state cross sections for process $H_2(c\,^3\Pi_u,\nu_i)+e\rightarrow H_2(g\,^3\Sigma_g^+,\nu_f)+e$ (solid lines) as a function of final vibrational quantum number, at the incident energy $E=10$ eV, for $\nu_i=0$, 6, and 13, compared with corresponding structural factors [Eq. (2)] (dashed lines) normalized to the first ν_f cross-section value.

Same considerations hold for the other two cases. Figures 11 and 12 show the cross sections for the $a\,^3\Sigma_g^+\rightarrow d\,^3\Pi_u$ and $c\,^3\Pi_u\rightarrow h\,^3\Sigma_g^+$ transitions, respectively, as a function of the final vibrational quantum number at an incident energy of 10 eV and for $\nu_i=0$, 6, 13. For $\nu_i=13$ the cross sections are shown only for $\nu_f\geqslant 3$ (and for $\nu_f\geqslant 2$ in Fig. 10), for which a vibrational excitation occurs: for $\nu_f<3$ ($\nu_f<2$ in Fig. 10), in fact, the transition energy is found to be negative.

V. DISCUSSION

The development of collisional-radiative models for H_2 plasmas [11,12] used as diagnostic tool for the determination of electronic and vibrational temperature of $H_2(X\,^1\Sigma_g^+)$ molecules requires the knowledge of vibrational population of all the triplet states correlating with $n=2$ and $n=3$ asymptotic states. An accurate model, therefore, must include all the direct and indirect processes, and their possible

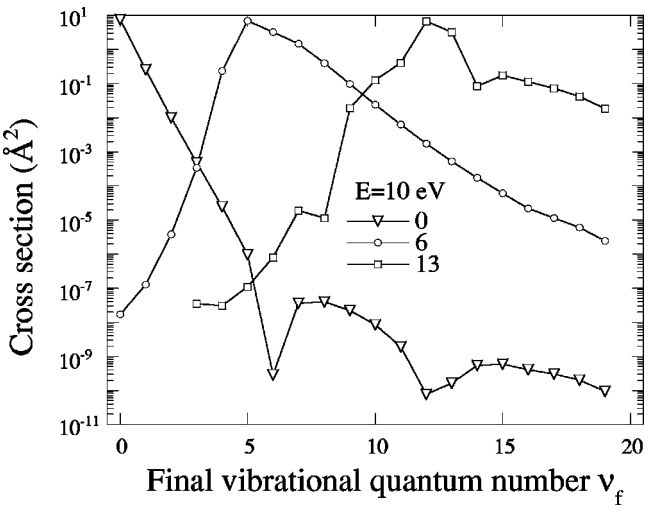

FIG. 11. State-to-state cross sections for process $H_2(a\,^3\Sigma_g^+,\nu_i)+e\rightarrow H_2(d\,^3\Pi_u,\nu_f)+e$ as a function of final vibrational quantum number, at the incident energy $E=10$ eV, for $\nu_i=0$, 6, and 13.

ramifications, which can affect the vibrational density. Such an analysis is complex and beyond the scope of present work. However, a brief qualitative discussion of the possible exit channels following the electron-impact excitation involving the triplet states considered here could be of interest and could provide indications for further quantitative studies.

Direct dissociative cross sections calculated in this paper refer to the electron-impact excitation to the repulsive branch of the upper *d*, *h*, and *g* potential curves, lying above the dissociation limit. Other processes however can lead to dissociation via indirect mechanisms. The $h\,^3\Sigma_g^+$ state, for instance, is coupled by symmetry with the completely repulsive state $b\,^3\Sigma_u^+$ and, in addition, supports a number of resonant vibrational states ($\nu'=4,5,6$, see below). These two circumstances can lead competitively to dissociation via radiative decay and tunneling effect, respectively. Wouters

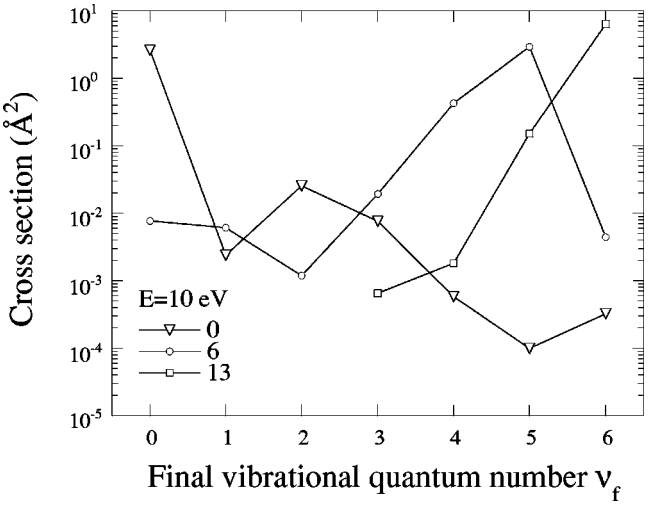

FIG. 12. State-to-state cross sections for process $H_2(c\,^3\Pi_u,\nu_i)+e\rightarrow H_2(h\,^3\Sigma_g^+,\nu_f)+e$ as a function of final vibrational quantum number, at the incident energy $E=10$ eV, for $\nu_i=0$, 6, and 13.

et al. [31] report, in an experimental-theoretical work, that the percentage of dissociative tunneling from the rotational levels of $\nu'=4$ vibrational state is in the range 0.1–8 % of the total (tunneling + radiative decay). In addition, in the above percentage the authors include also the contribution coming from predissociation of *h* state via $a\,^3\Sigma_g^+$ and $i\,^3\Pi_g$ states. They found completely different results for the rotational levels of $\nu'=5$ quasibound state, which mostly dissociates by tunneling (80%). These results indirectly confirm our calculations. Actually, as discussed below, the tunneling dissociative cross section for the $\nu'=5$ resonant level of $h\,^3\Sigma_g^+$ electronic state is found to be much higher than the corresponding cross section for the $\nu'=4$ level, due to the short tunneling lifetime of $\nu'=5$ resonant state which allows the barrier penetration before radiative decay to $c\,^3\Pi_u$ state might occur. The inverse situation has been found for $\nu'=4$ case.

The $d\,^3\Pi_u$ state can radiatively decay back to the $a\,^3\Sigma_g^+$ state, but also undergo predissociation through the $b\,^3\Sigma_u^+$ triplet state. The cumulative lifetime for these two processes has been measured and calculated by Kiyoshima *et al.* [24]. Furthermore, the higher vibrational levels ($\nu_f>6$) of *d* state lie above the ground vibrational level of H_2^+ molecular ion, and the excitation to these levels can lead to autoionization. No quantitative information exists, to the best of our knowledge, on this process, which affects directly the population of *d* state, and, thereby, the results of Fulcher band emission in divertor plasma diagnostic [11,12]. Autoionization, finally, can also occur from the high vibrational levels ($\nu_f>6$) of the $g\,^3\Sigma_g^+$ electronic state.

As mentioned in Sec. III A, the energy positions of quasibound vibrational levels in the $h^3\Sigma_g^+$ electronic state were determined by evaluating the IA by Eq. (12). The plot of the IA against the continuum energy ε, shown in Fig. 2, displays three sharp peaks of very narrow amplitude (the inserted picture in Fig. 2 shows the dependence of the second resonance on the continuum energy at a closer scale) whose maximum is placed, with respect to the bottom of the ground-state potential well, at the energies of 121 038.85, 122 357.89, and 123 325.99 cm^{-1} correspondingly. In particular, in the first two energy regions, the amplitude of the $\chi_\varepsilon(R)$ wave functions is very high inside the potential well and rapidly decays under the barrier, becoming finally oscillating as the internuclear distance tends to infinity. This can be better seen in Fig. 13 where the $\chi_\varepsilon(R)$ wave function is shown for the three different values of energy (full lines), corresponding to the maximum of the three peaks in Fig. 2, along with the vibrational wave function for an ε value falling outside the resonance regions (dashed line). In the figure, the amplitudes of the first two quasibound wave functions, inside the well, are reduced by a factor of 10^{-6} and 10^{-2}, respectively, while the dashed curve is magnified by a factor of 10^5, for a better representation. This figure suggests that the tunneling probability for the first resonance should be very small, due to the very large amplitude of $\chi_\varepsilon(R)$ inside the potential well, compared with the amplitude beyond the barrier.

The situation for the third resonant region in Fig. 2 is quite different. In this case the peak of the internal amplitude

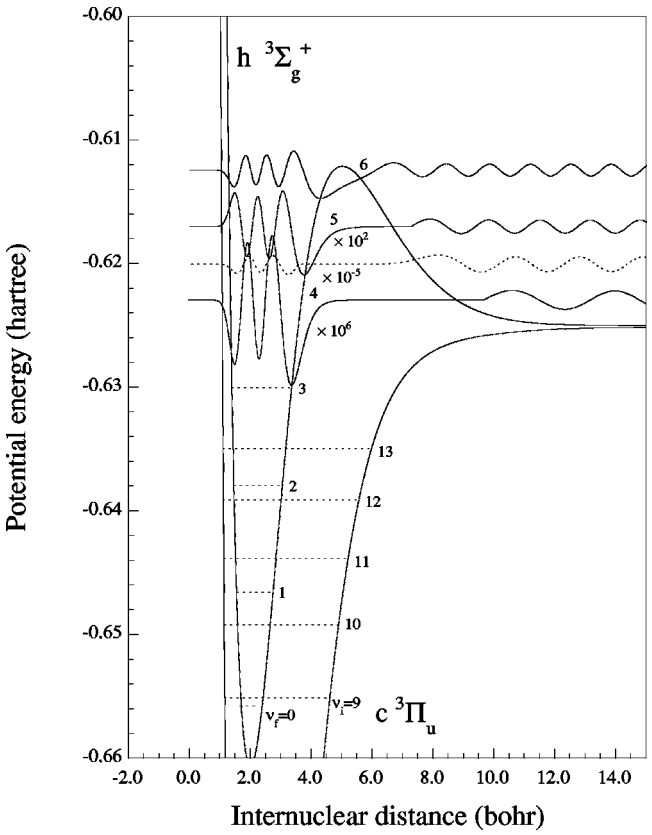

FIG. 13. Potential-energy curves and vibrational levels for $c\,^3\Pi_u$ and $h\,^3\Sigma_g^+$ states of H_2. Some wave functions of quasibound states (corresponding to internal amplitude peaks) (full lines) and for a non-quasi-bound level (dashed line) are also displayed. The left portion of the first three wave functions (from the origin of the internuclear distance to the right wall of the barrier) has been multiplied by 10^{-6}, 10^5 (dashed line), and 10^{-2} for a better representation.

is placed close to the top of the barrier, near the pure continuum vibrational spectrum, so a more pronounced dissociative character of this quasibound vibrational level is to be expected. The small barrier height and width, in fact, ensure a high tunneling probability. Finally, an intermediate situation is found for the second resonance region, where the wave-function amplitude for the vibrational level reaches intermediate values with respect to the other two cases (Fig. 13).

No contribution from direct dissociation is to be expected from quasibound levels, due to the small vibrational overlap in the region of internuclear separation, behind the barrier, where the vibrational wave function for the bound levels of $c\,^3\Pi_u$ state rapidly vanishes (see Fig. 13). A similar situation can be predicted for those levels lying outside the resonance regions. In this case the corresponding wave functions exhibit large oscillations only in the asymptotic region (dashed line in Fig. 13), which implies again a weak overlap in the Franck-Condon integral. Direct dissociation from the pure vibrational continuum above the potential barrier can, however, be quite significant.

The last feature of the quasibound vibrational wave functions we want to stress is that although they have, rigorously speaking, a continuum nature, due to a nonzero amplitude behind the potential barrier, and their amplitude inside the potential well changes significantly through the resonance shape, the nodes, conversely, remain unperturbed and their number progressively increases from four through six passing from the first to the third peak. This allows the characterization of the three resonance levels by a pseudoquantum number $\nu'=4,\ 5,\ 6$.

The tunneling of all these three states is obviously (in the frame of two-state transition) in competition with the radiative decay back to the $c\,^3\Pi_u$ vibrational manifold. The dissociative cross sections for the excitation to the quasibound states can be thus calculated only when the *relative tunneling probability* is known. We have defined the tunneling branching ratio P in terms of the resonance lifetime τ_d [Eq. (13)] and radiative decay time τ_r [Eq. (18)] as

$$P(\varepsilon)=\frac{\tau_d^{-1}(\varepsilon)}{\tau_d^{-1}(\varepsilon)+\tau_r^{-1}(\varepsilon)}. \tag{17}$$

The radiative lifetime is defined through the Einstein coefficients of spontaneous emission,

$$\tau_r=\frac{1}{\sum_{\nu_i} A(\nu',\nu_i)+\int d\varepsilon'\dfrac{dA(\nu',\varepsilon')}{d\varepsilon'}}, \tag{18}$$

where ε' is the continuum energy levels for the initial electronic state $c\,^3\Pi_u$.

The Einstein coefficient for a quasibound level which radiatively decays to a bound level is given by

$$A(\nu',\nu_i)=\int_{\varepsilon_{min}}^{\varepsilon_{max}} d\varepsilon\, 2.142\times 10^{10} \times(\varepsilon-\varepsilon_{\nu_i})^3 g|\langle\chi_\varepsilon|M(R)|\chi_{\nu_i}\rangle|^2, \tag{19}$$

where ε_{min} and ε_{max} are the energy limits of the resonance shape and g is a symmetry factor depending on the transition. For radiative decay to the continuum of the lower state the expression of the Einstein coefficient $A(\nu',\varepsilon')$ involves a double integral over the energy.

We have estimated the radiative decay considering only that portion of the wave function trapped in the potential well, so that all integrals on R were truncated under the barrier. The resonance lifetime was estimated by using the WKB approximation [Eq. (13)]. In the case of the second resonance $(\nu'=5)$, however, we have checked the accuracy of the semiclassical approximation by calculating the resonance lifetime through the time delay τ [26,32], defined as

$$\tau(\varepsilon)=\int_0^\infty(\chi_\varepsilon^*\chi_\varepsilon-\chi_\infty^*\chi_\infty)dR+\left(\frac{\mu}{\hbar k^2}\right)\sin(2\delta_\varepsilon), \tag{20}$$

where δ_ε is the *phase shift* and $k^2=2\mu\varepsilon/\hbar^2$. The exact radial wave function is asymptotically normalized as

TABLE I. Tunneling, τ_d, and radiative decay, τ_r, lifetimes.

ν'	τ_d (s)	τ_r (s)
4	1.0	9.1×10^{-8}
5	3.5×10^{-9}	1.0×10^{-7}
6	1.3×10^{-13}	1.2×10^{-7}

$$\chi_\varepsilon \simeq \chi_\infty, \quad R\to\infty$$
$$\chi_\infty \equiv \left(\frac{2\mu}{\pi\hbar^2 k}\right)^{1/2} \sin(kR+\delta_\varepsilon). \tag{21}$$

The resonance lifetime is correlated to the time delay by [26]

$$\tau_d = \tfrac{1}{4}[\tau]_{max}. \tag{22}$$

We have evaluated τ at the energy peak ε_{max} for the level $\nu'=5$, finding the value of 3.48×10^{-9} s, in good agreement with the semiclassical value of 3.52×10^{-9} s.

Table I gives the numerical values of τ_d and τ_r. As it can be seen from this table, for the first case ($\nu'=4$) $\tau_d \gg \tau_r$, which implies $P\approx 0$, confirming the strong bound nature of this level. For the next two levels ($\nu'=5,6$), the tunneling probability is appreciably different from zero.

The cross sections for dissociation via the excitation to the resonant levels can be obtained by using the expression

$$\sigma_{\nu_i}(E) = \int_{\varepsilon_{th}}^{\varepsilon_{top}} P(\varepsilon)\frac{d\sigma_{\nu_i,\varepsilon}(E)}{d\varepsilon}d\varepsilon, \tag{23}$$

where ε_{th} and ε_{top} represent the continuum energy threshold and the maximum value of the potential barrier, respectively. The integration in Eq. (23) has been performed only for the three narrow regions, labeled as $\nu'=4,5,6$, where the internal amplitude is markedly different from zero. P has been assumed as independent of the continuum energy by setting its value at the energy peak position ε_{max}. The dissociative cross sections obtained are shown in Fig. 14. The curve for the first resonance ($\nu'=4$), which is magnified by a factor of 10^7, confirms the almost nondissociative character of this level. The second ($\nu'=5$) and third ($\nu'=6$) resonances give, however, a non-negligible contribution to the dissociation for $3\leqslant\nu_i\leqslant 10$ and $\nu_i\gtrsim 6$, respectively. All these results have been included in the total cross sections shown in Fig. 7(a).

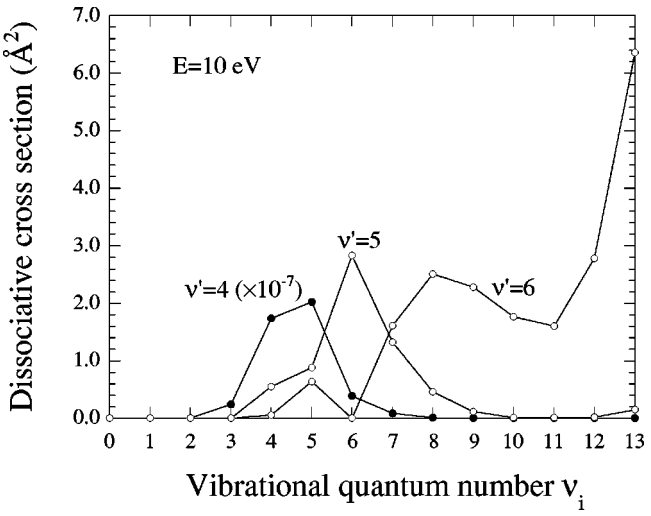

FIG. 14. Quasibound state dissociative cross section for the process $H_2(c\,^3\Pi_u,\nu_i)+e\to H_2(h\,^3\Sigma_g^+,\nu')+e$ as a function of initial vibrational quantum number, at the incident energy $E=10$ eV. The curve labeled as $\nu'=4$ has been multiplied by a factor of 10^7.

VI. CONCLUSIONS

We have calculated the electron-impact cross section for the transitions $a\,^3\Sigma_g^+\to d\,^3\Pi_u$, $c\,^3\Pi_u\to h\,^3\Sigma_g^+$, and $c\,^3\Pi_u\to g\,^3\Sigma_g^+$ using the impact-parameter method. No other theoretical or experimental data exist for these transitions, to the best of our knowledge, to which the present results can be compared. As expected, the small energy difference between the initial and the final electronic states involved in these transitions results in cross sections that are much (one-to-two orders of magnitude) larger than previously studied singlet-singlet transitions induced in $H_2(X\,^1\Sigma_g^+,\nu_i)$ by electron impact. Due to space limitations, only total, dissociative and some $\nu_i-\nu_f$ resolved cross sections are presented. The entire set of data is available on request from the authors [33].

ACKNOWLEDGMENTS

This work was partially supported by ASI (Contract No. I/R/055/02) and MIUR (Project No. 2001031223_009). The authors wish to thank Professor M. Capitelli and Dr. G. Colonna for useful discussions.

[1] *Proceedings of Atomic and Molecular Processes in Divertor Plasma Volume Recombination*, edited by R.K. Janev and D.R. Schultz [Phys. Scr. **T96** (2002)].

[2] M. Capitelli, R. Celiberto, and M. Cacciatore, in *Advances in Atomic, Molecular and Optical Physics*, edited by M. Inokuti (Academic Press, New York, 1994), Vol. 33, p. 321.

[3] R. Celiberto, R.K. Janev, A. Laricchiuta, M. Capitelli, J.M. Wadehra, and D.E. Atems, At. Data Nucl. Data Tables **77**, 1 (2001).

[4] R. Celiberto, M. Capitelli, N. Durante, and U.T. Lamanna, Phys. Rev. A **54**, 432 (1996).

[5] R. Celiberto, M. Cacciatore, M. Capitelli, and C. Gorse, Chem. Phys. **133**, 355 (1989).

[6] R. Celiberto, P. Cives, M. Cacciatore, M. Capitelli, and U.T.

Lamanna, Chem. Phys. Lett. **169**, 69 (1990).
[7] D.T. Stibbe and J. Tennyson, New J. Phys. **1**, 2.1 (1998).
[8] C.S. Trevisan and J. Tennyson, Plasma Phys. Controlled Fusion **44**, 2217 (2002).
[9] T.N. Rescigno and B.I. Schneider, J. Phys. B **21**, L691 (1988).
[10] S. Chung, C.C. Lin, and E.T.P. Lee, Phys. Rev. A **12**, 1340 (1975).
[11] U. Fantz and B. Heger, Plasma Phys. Controlled Fusion **40**, 2023 (1998).
[12] U. Fantz, B. Heger, and D. Wunderlich, Plasma Phys. Controlled Fusion **43**, 907 (2001).
[13] A.U. Hazi, Phys. Rev. A **23**, 2232 (1981).
[14] M.J. Redmon, B.C. Garrett, L.T. Redmon, and C.W. McCurdy, Phys. Rev. A **32**, 3354 (1985).
[15] B.C. Garrett, L.T. Redmon, C.W. McCurdy, and M.J. Redmon, Phys. Rev. A **32**, 3366 (1985).
[16] R. Celiberto and T.N. Rescigno, Phys. Rev. A **47**, 1939 (1993).
[17] R. Celiberto, U.T. Lamanna, and M. Capitelli, Phys. Rev. A **50**, 4778 (1994).
[18] R. Celiberto, A. Laricchiuta, U.T. Lamanna, R.K. Janev, and M. Capitelli, Phys. Rev. A **60**, 2091 (1999).
[19] S. Geltman, *Topics in Atomic Collision Theory* (Academic Press, New York, 1969), p. 192.
[20] G. Staszewska and L. Wolniewicz, J. Mol. Spectrosc. **198**, 416 (1999).
[21] M.W. Schmidt, K.K. Baldridge, J.A. Boatz, S.T. Elbert, M.S. Gordon, J.H. Jensen, S. Koseki, N. Matsunaga, K.A. Nguyen, S. Su, T.L. Windus, M. Dupuis, and J.A. Montgomery, Jr., J. Comput. Chem. **14**, 1347 (1993).
[22] P.O. Widmark, P.A. Malmqvist, and B. Roos, Theor. Chim. Acta **77**, 291 (1990).
[23] Basis sets were obtained from the Extensible Computational Chemistry Environment Basis Set Database, Version 6/28/02, as developed and distributed by the Molecular Science Computing Facility, Environmental and Molecular Sciences Laboratory, which is part of the Pacific Northwest Laboratory, P.O. Box 999, Richland, WA 99352, USA, and funded by the U.S. Department of Energy. The Pacific Northwest Laboratory is a multiprogram laboratory operated by Battelle Memorial Institue for the U.S. Department of Energy under Contract No. DE-AC06-76RLO 1830. Contact David Feller or Karen Schuchardt for further information.
[24] T. Kiyoshima, S. Sato, S.O. Adamson, E.A. Pazyuk, and A.V. Stolyarov, Phys. Rev. A **60**, 4494 (1999).
[25] I. Drira, J. Mol. Spectrosc. **198**, 52 (1999).
[26] R.J. Le Roy and R.B. Bernstein, J. Chem. Phys. **54**, 5114 (1971).
[27] R.J. Le Roy and Wing-Ki Liu, J. Chem. Phys. **69**, 3622 (1978).
[28] G. Colonna, Rend. Circ. Mat. Palermo **57**, Suppl. 2, 159 (1998).
[29] W.H. Miller, J. Phys. Chem. **83**, 960 (1979).
[30] R. Celiberto, M. Capitelli, and R.K. Janev, Chem. Phys. Lett. **256**, 575 (1996).
[31] E.R. Wouters, B. Buijsse, J. Los, and W.J. van der Zande, J. Chem. Phys. **106**, 3974 (1997). We have adopted the denomination established by Wolniewicz *et al.* in Ref. [20] for the nomenclature of H_2 triplet states. Wouters *et al.* use a different identification. In particular, the *g* and *h* states in their work correspond to *h* and *g* states, respectively, in the present paper.
[32] F.T. Smith, Phys. Rev. **118**, 349 (1960); **119**, 2098(E) (1960).
[33] cscpal38@area.ba.cnr.it